atoms

MDPI

Article

Spectral and Divergence Characteristics of Plateau High-Order Harmonics Generated by Femtosecond Chirped Laser Pulses in a Semi-Infinite Gas Cell

Stylianos Petrakis [1,2], Makis Bakarezos [2,3], Michael Tatarakis [2,4], Emmanouil P. Benis [1,*] and Nektarios A. Papadogiannis [2,3]

[1] Department of Physics, University of Ioannina, 45110 Ioannina, Greece; spetrak@hmu.gr
[2] Institute of Plasma Physics and Lasers, Hellenic Mediterranean University Research Centre, 74100 Rethymno, Greece; bakarezos@hmu.gr (M.B.); mictat@hmu.gr (M.T.); npapadogiannis@hmu.gr (N.A.P.)
[3] Department of Music Technology and Acoustics, Hellenic Mediterranean University, 74133 Rethymno, Greece
[4] Department of Electronic Engineering, Hellenic Mediterranean University, 73133 Chania, Greece
* Correspondence: mbenis@uoi.gr

Abstract: The generation of high-order harmonics in a semi-infinite cell by femtosecond laser pulses is a common practice for reliable coherent and low divergence XUV source beams for applications. Despite the relative simplicity of the experimental method, several phenomena coexist that affect the generated spectral and divergence characteristics of the high harmonic XUV frequency comb. The ionisation degree of the medium and the consequent plasma formation length imposes a spatiotemporal evolution of the fundamental EM field and XUV absorption. Varying the laser pulse chirp and the focusing conditions, as well as the gas density, we measured intense harmonic spectral and divergence variations attributed mainly to self-phase modulations of the laser EM field in the partially ionised medium. Additionally, low-divergence high harmonics are observed for certain laser chirp values attributed to the strong phase matching of only the short electron quantum path. Thus, a tunable, low divergent, and coherent XUV source can be realised for spatiotemporal imaging applications in the nanoscale.

Keywords: high-order harmonic generation; self-phase modulation; semi-infinite cell; chirped laser pulses

Citation: Petrakis, S.; Bakarezos, M.; Tatarakis, M.; Benis, E.P.; Papadogiannis, N.A. Spectral and Divergence Characteristics of Plateau High-Order Harmonics Generated by Femtosecond Chirped Laser Pulses in a Semi-Infinite Gas Cell. *Atoms* **2022**, *10*, 53. https://doi.org/10.3390/atoms10020053

Academic Editor: Alexander Kramida

Received: 4 April 2022
Accepted: 17 May 2022
Published: 24 May 2022

1. Introduction

Many modern laser laboratories worldwide are equipped with femtosecond laser systems and related technology, routinely delivering mJ pulses at kHz repetition rates. The interaction of these strong field pulses with atomic gaseous targets results in the generation of coherent XUV radiation in the form of a comb of odd-order harmonics of the laser field fundamental frequency. This coherent XUV radiation, that propagates along the direction of the laser beam, may serve as a secondary source for applications related to imaging techniques based on coherent diffraction imaging (CDI) [1–4]. The necessity for development of such secondary coherent XUV sources, with high-quality spectral and geometrical characteristics, has been recently emphasised [5]. The XUV quality is governed primarily by the laser pulse characteristics (peak intensity, temporal frequency, and phase) as well as the atomic gas target (Coulombic well and gas pressure). Thus, a thorough understanding of the dynamics of the coherent XUV radiation, known as high-order harmonic generation (HHG), in respect to these parameters is required for further improving such secondary sources.

The HHG process can be adequately described within the three-step model concept [6,7]. In this picture, the first step is the ionisation of the atomic target by the strong laser electric field primarily via tunnelling ionisation [8]. In the second step, the emitted electron

follows quantum paths in the strong alternating laser electric field that may result in a recollision with the parent ion. In the third step, upon recollision, the excess of the electron energy is emitted as high-frequency radiation. This recollision mechanism is repeated every half-period of the laser field, thus resulting in the formation of a comb of odd-order harmonics. The macroscopic coherent addition of the generated XUV radiation, driven by quasi-phase matching conditions [9–11], forms the secondary coherent XUV beam, which propagates along with the laser beam, as shown in Figure 1. The HHG spectrum structure initially exhibits a decrease (lower order harmonics), followed by an extended region of harmonics with approximately the same efficiency (plateau), and finally a region where the harmonics signal rapidly decreases (cut-off).

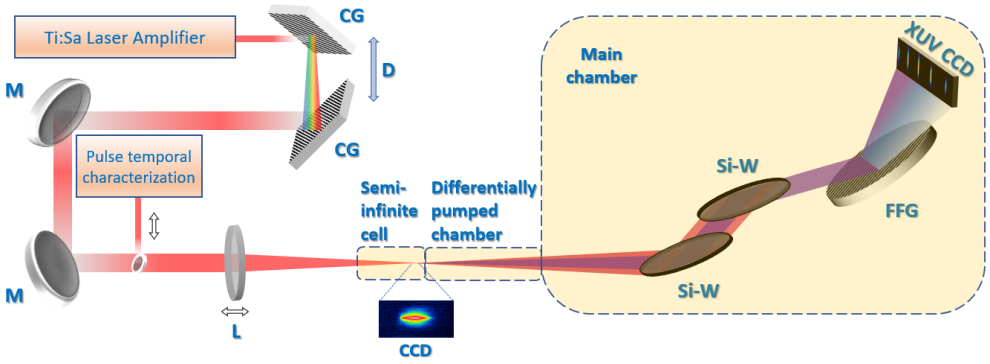

Figure 1. Schematic layout of the HHG experimental setup. Femtosecond IR Ti:Sa laser pulses, chirped by varying the spacing between the compressor gratings (CG), are focused on a semi-infinite Ar gas cell generating coherent XUV harmonic radiation. The XUV beam propagates collinearly with the IR laser beam to the third stage of the setup, where the IR is filtered by two silicon wafers (Si-W). The XUV beam is then dispersed by a flat-field XUV concave grating (FFG) and the plateau XUV harmonics spectra and divergence are imaged by an XUV CCD camera. D: Adjustable grating distance; M: low dispersion fs mirror; L: low dispersion thin-focusing lens. The plasma formation inside the semi-infinite gas cell is imaged by a CCD camera.

The HHG spectral and divergence characteristics, manifesting the quality of the coherent XUV source, depend on the dynamic response of the generation process both at the atomic level as well as at a macroscopic level. At the atomic level, it is known that for the same electron-return energy, there are only two surviving quantum paths that result in a recollision with the parent ion during the first laser cycle [7]. One of the paths lasts for a shorter time than the other, and are termed as *short* and *long* trajectories, respectively. The main distinctive footprint of the two trajectories in each plateau harmonic is the difference in their divergence, owed to the difference in travel time in the generating medium [12]. The qth-order harmonic signal results from the coherent summation of the aforementioned quantum paths and corresponds to an energy of $E = q\hbar\omega_{L0}$, where ω_{L0} is the laser central frequency. Thus, the temporal characteristics of the plateau harmonics depend strongly on the phase difference between the long and short trajectories, which also depends on the time-dependent laser intensity [13].

At a macroscopic level, the coherent addition of the generated harmonics in each laser half-cycle is evolving. However, this coherent addition is affected by propagation effects due to the inherent laser beam phase shifts (Gouy phase) and the variation of the refractive index in the atomic gas target, as well as the plasma formed by the partially ionised medium. Moreover, in conditions of strong laser pulses, the laser field may suffer variations in respect to the temporal arrangement of its spectral content (chirp), and consequently to its pulse duration and temporal intensity, resulting from mechanisms known as self-phase modulation (SPM) owed to the Kerr effect in the atomic gas, as well as in the rapidly ionised medium (plasma) [14]. SPM effects, depending on their strength,

may result in spectra lines shifting and broadening that significantly affect the HHG spectra and their divergence.

From the above, it becomes evident that the quality of the HHG source, in terms of the geometrical and phase characteristics of the harmonics beam, depends strongly on the temporal characteristics of the long and short trajectories, as well as on the SPM effects. Thus, developing methods for controlling the relevant contribution of long and short trajectories of the plateau harmonics, and the role of the SPM effects, is of fundamental significance. Recently, we reported on such a proof-of-principle method for the coherent control of the two quantum paths in plateau harmonics generated in a noble gas, based on the accurate control of the laser pulse chirp variation [15]. The latter allowed for the accurate control of the time-dependent slope of the cycle-averaged laser intensity, the temporal evolution of the ionisation degree of the medium, and the SPM of the laser pulse inside the partially ionised medium. Specifically, we reported on experimental conditions under which the efficiency of the generation of the two trajectories could be controlled, even having the short trajectory as the only surviving one.

In this article, we present a thorough systematic study of the spectral and divergence characteristics of the plateau harmonics generated in an Ar-filled semi-infinite gas cell, at various gas pressures and laser beam focal conditions, as a function of the chirp imposed to the laser pulses. Based on this, we were able to monitor the evolution of the plateau HHG spectra and their divergence from positive to negative chirp values for increasing gas pressures. Our findings indicate that, for these high laser intensity conditions, the maximum HHG signal is obtained for negatively chirped pulses close to the Fourier-transform-limited (FTL) value of the laser pulses, even for gas pressures as small as 30 Torr, where the HHG signal is much smaller outside the aforementioned chirp region. Interestingly, for high pressures, additional and broader lines start to appear in the HHG spectra, which then resemble a quasi-continuum spectrum. This feature is of significant importance, since the secondary coherent-HHG source can be easily tuned to denser-spaced wavelengths for these generation conditions. In addition, the contribution of the long and short trajectories to the HHG spectra, evident by their divergence, is monitored with the smooth variation of the chirp. Even though similar investigations exist in the literature [16,17], these report only HHG spectra, unlike our work where we record both the HHG spectra and the HH divergence simultaneously, the latter being a fine tool for investigating the delicate dynamics behind the HHG and the role of the short and long trajectories in it. Phenomenological model calculations [15], which take into account the aforementioned physical processes, accompany our experimental findings on the spectral characteristics of the generated harmonics.

2. The Experimental Setup

A schematic layout of our experimental setup, developed at the Institute of Plasma Physics and Lasers (IPPL) [18], is shown in Figure 1. The setup consists of three stages connected in line. The first stage is a semi-infinite static cell that contains the generating gas at pressures ranging from 30 to 90 mbar for the current study. The second stage is a differentially pumped chamber, necessary for separating the high-pressure first stage from the third low-pressure stage. The second stage is pumped by a 150 L/s turbomolecular pump reaching vacuum values of the order of 10^{-4} mbar when the gas cell is operating. The third stage is a 70 cm-diameter chamber pumped by a 350 L/s turbomolecular pump reaching a background pressure of 1×10^{-6} mbar. The chamber hosts the optical setup for filtering and recording the image traces of the generated XUV harmonic radiation.

The IR laser pulses, having a nominal central wavelength of 807 nm, are delivered by the Ti:Sa laser system (Amplitude Technologies) to the experimental station with an energy of 1 mJ and a variable pulse duration, the FTL (i.e., the shortest possible) value of which is 26 fs. The pulse duration is accurately controlled by varying the distance between the compressor's gratings of the laser amplifier relative to the position which delivers FTL laser pulses. Thus, positively or negatively chirped laser pulses are routinely

delivered to the experimental station for measurements. Assuming only linear chirp, its value is experimentally estimated in shot-to-shot basis via a femtosecond single-shot intensity autocorrelator (Amplitude Technologies, Bonsai) just before the interaction cell. The distance of the gratings in the laser compressor can be tuned according to the measured pulse duration and thus the laser pulse chirp is fully controlled during the experiments.

The laser beam is focused by a 38 cm focal distance lens at the exit pinhole area of the semi-infinite static cell filled with Ar gas at appropriate pressures. The interaction of the intense laser electric fields with the Ar atoms results in the generation of an XUV comb of harmonics that propagates along with the laser beam to the third stage of the setup. There, it is initially filtered from the IR using a pair of Si wafers placed at the Brewster angle for the IR and then it is diffracted by the grazing-incidence flat-field diffraction grating (Hitachi 001-0639) allowing for high angular dispersion efficiency for the harmonics from 22 nm to 124 nm. The XUV light is detected at the focal plane of the harmonics of interest ($15\omega_{L0}$–$23\omega_{L0}$) using a high quantum efficiency 16-bit X-ray vacuum CCD camera (Raptor Photonics, Eagle XO) with a sensor having 2048 pixels (27.65 mm) at the grating diffraction axis and 512 pixels (6.90 mm) at the XUV divergence axis (perpendicular to the grating diffraction axis). The XUV grating and detector allow for a relatively high spectroscopic resolution from ∼80 to ∼100 pixels per 1 nm on the CCD for the spectral region of interest. This resolution is a significant experimental tool for the observations presented here. Finally, the plasma formation inside the semi-infinite gas cell is imaged by a CCD camera for all the corresponding XUV images. In our study, plasma images are indispensable for the interpretation of the corresponding XUV spectral and divergent characteristics.

3. Results

The findings of our study are summarised in Figures 2 and 3, where the spectral images of the plateau harmonics, $15\omega_{L0}$–$23\omega_{L0}$, accompanied by their corresponding plasma formation images, are systematically recorded as a function of the laser pulse chirp for Ar gas pressures ranging from 30 to 90 Torr. In Figure 2, the focus of the laser beam is at the exit pinhole ($\sim$ 100 μm in diameter) of the semi-infinite cell, while in Figure 3, it is 3 mm before the exit pinhole. Both sets of measurements were performed maintaining a constant laser pulse energy of 1.0 mJ, as well as the same focusing conditions, i.e., f-number = 4. The laser peak intensity for the FTL pulse of 26 fs was experimentally estimated to be $2.3 \pm 0.5 \times 10^{15}$ W/cm^2, which is far above the ionisation saturation intensity for Ar [15]. The pulse durations, indicated in the spectral images in Figures 2 and 3 with plus and minus signs, correspond to the positive (instantaneous frequency increasing with time) and negative (instantaneous frequency decreasing with time) chirp values, respectively. The colour-code scale in Figures 2 and 3 was kept identical for both XUV spectral and plasma images for comparison purposes. The main features that are readily observed in the images are the following:

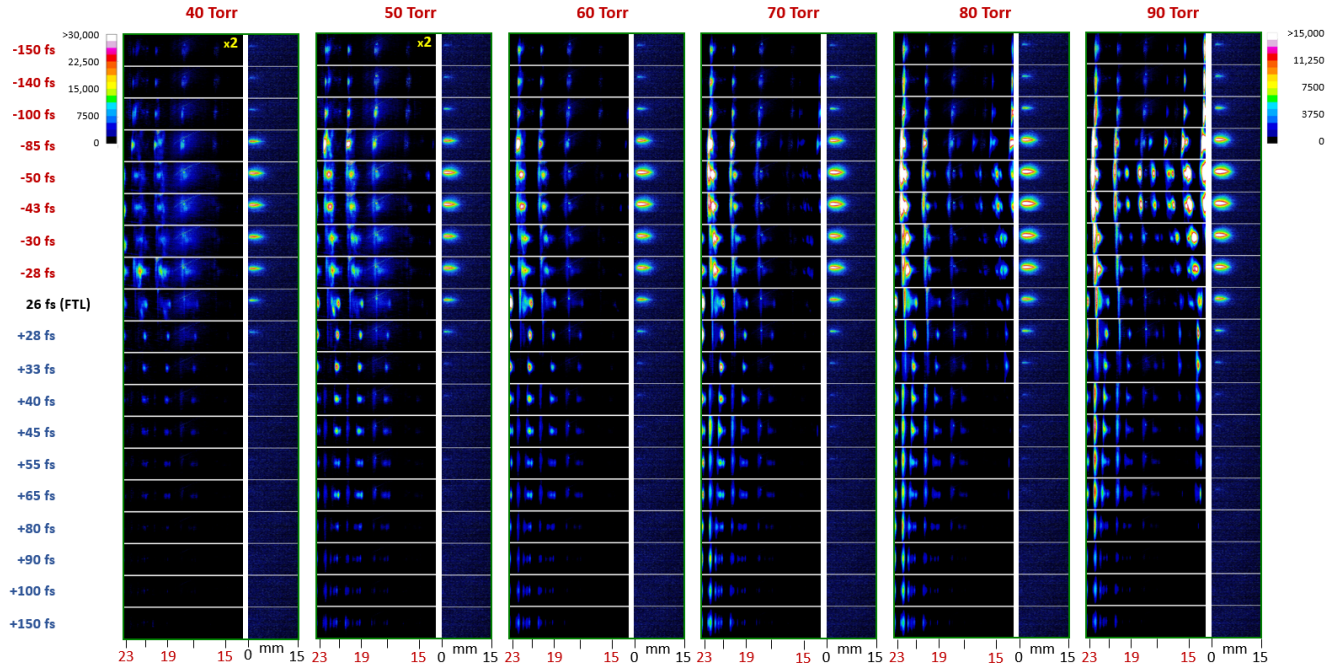

Figure 2. XUV harmonic spectral images (**left**) and corresponding plasma formation images (**right**) measured for various laser pulse durations and Ar gas pressures in the semi-infinite cell. The focus of the laser beam is at the exit pinhole of the semi-infinite cell. The negative/positive signs of the laser pulse durations correspond to the imposed negative/positive chirp, respectively. The nominal spectral locations of the harmonics order, estimated according to the optical geometry of the experimental setup, are noted at the bottom of the XUV spectral images for each gas pressure. The colour intensity of the XUV spectral images corresponding to the pressures of 40 and 50 Torr was multiplied by a factor of two, as indicated at the top of the images, for better visibility.

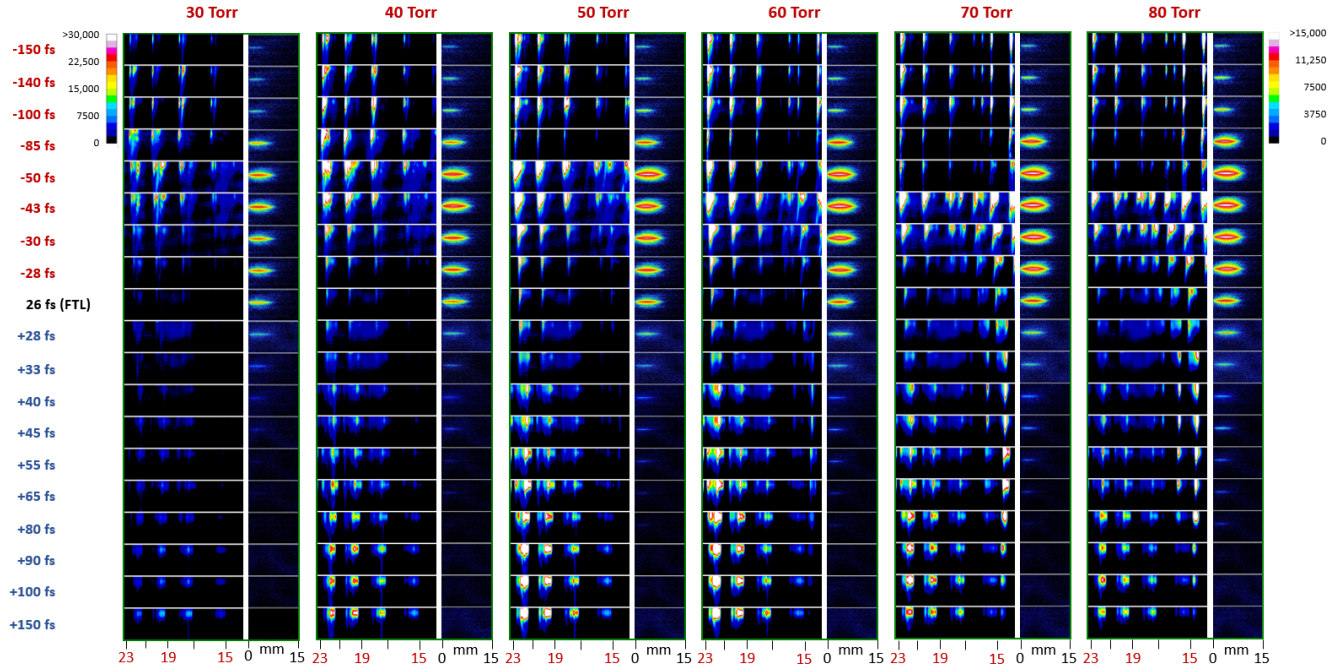

Figure 3. Same as in Figure 2, except that the focus of the laser beam is 3 mm before the exit pinhole of the semi-infinite cell.

Line broadening and quasi-continuum spectra. For low negative chirp values (<−50 fs), the plateau HHG signal is markedly enhanced, even for Ar gas pressures as low as 30 Torr, while at the same time, the harmonic lines suffer a considerable spectral broadening. Moreover, at high-value gas pressures (90 Torr in Figure 2 and larger than 60 Torr in Figure 3), additional spectral bands appear in between the spectral locations of the plateau harmonics. Thus, the resulting spectrum resembles a quasi-continuum spectrum. This spectral behaviour is closely related to the increased degree of ionisation of the generating medium, as can be inferred from the corresponding plasma luminescence images. Indeed, this feature is absent for lower negatively (<−85 fs) or any positively chirped laser pulses, where the degree of ionisation is much smaller and the resulting HHG spectra are similar to typical plateau HHG spectra.

In order to quantify this behavior, we estimate the relative enhancement of the integrated measured XUV emission in the spectral bands between the locations of the harmonics. Specifically, we focused our study on the case of a −43 fs laser pulse duration in Figure 3, for which the overall XUV emission is seen to be maximised. The aforementioned spectral bands correspond to the bandwidths, $\Delta\lambda$, of 38.5–41.3, 42.4–45.4, 48.4–50.5, and 53.7–56.0 nm, as determined from the 30 Torr pressure XUV image. We determined the enhancement of the XUV emission for each band as the ratio of the integrated XUV emission for each pressure to the integrated XUV emission for the pressure of 30 Torr. The XUV signal of the latter is close to the detection limits of our system. Thus, the relative enhancement of the XUV band emission is obtained as a function of the generating gas pressure. The results, presented in Figure 4, clearly show an overall relative enhancement factor between 5 and 6 for the bands of 38.5–41.3, 42.4–45.4, and 48.4–50.5 nm. The band of 53.7–56.0 nm, however, shows an enhancement for pressures up to 60 Torr, which is followed by a reduction for higher pressures. This is attributed to the absorption of these wavelengths for high Ar density values, as can be inferred from reference [19].

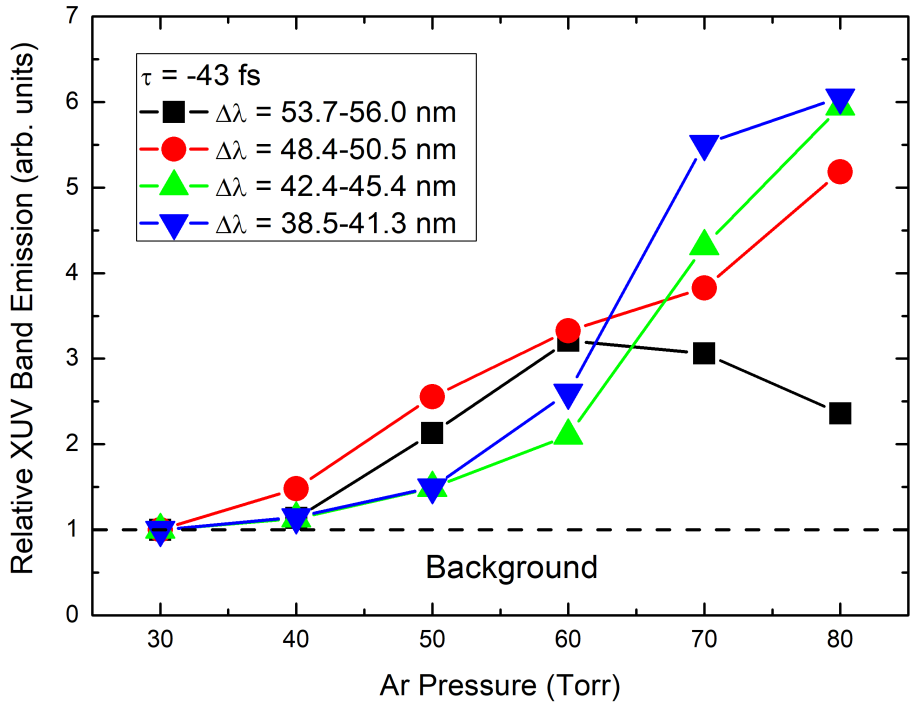

Figure 4. Relative enhancement of the measured XUV band emission for the spectral areas between the harmonics as a function of the generating gas pressure. The data correspond to those of Figure 3 for the pulse duration of τ = −43 fs. Relative XUV band emission error bars are estimated lower than 1% and are within the data symbols.

Harmonics divergence and quantum paths separation. A distinctive feature of the spectral images is the variation of the divergence of the plateau harmonics as the laser chirp is varied from positive to negative values. The feature is clearly seen in Figure 2, while it is less pronounced in Figure 3, where the higher and broader XUV emission smears out the divergence characteristics. A closer inspection of the spectral area of each harmonic in Figure 2 shows that it consists of two components that are attributed to the long and the short electron trajectory contributions, respectively. Their identification is determined by their different divergence, with the long trajectory presenting, in general, a higher divergence than the short trajectory [15]. Moreover, their spectral splitting is related to their inherent spectral blue shift, with the long trajectory suffering a stronger shift and thus appearing at shorter wavelengths [12]. Typically, the divergence of the 21st harmonic short and long trajectories as a function of the chirped laser pulse duration for the case of the 90 Torr Ar gas pressure of Figure 2 is presented in Figure 5 .

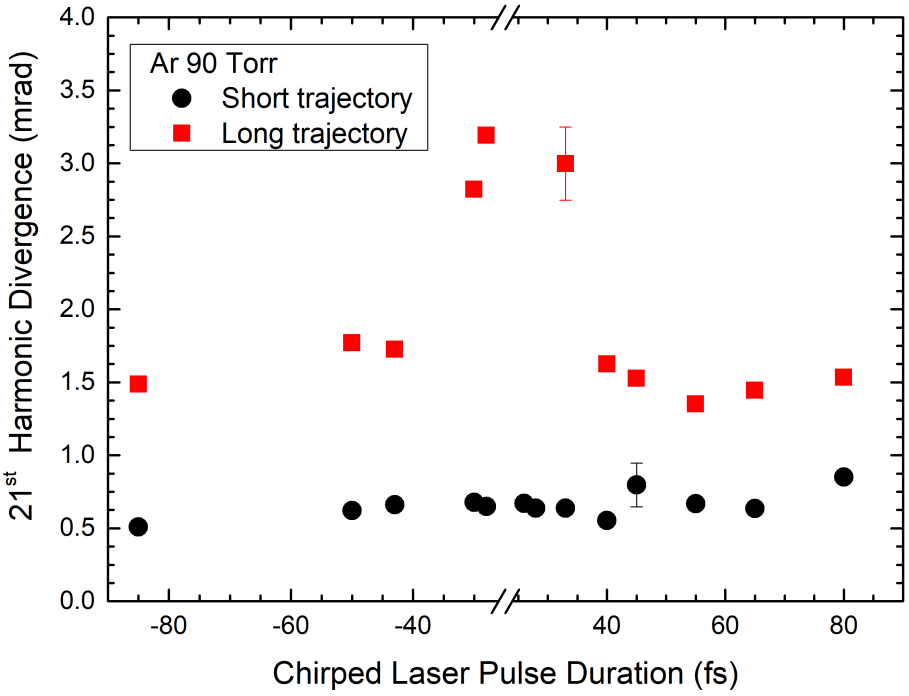

Figure 5. Experimentally determined divergence of the 21st harmonic short (black solid circle) and long (red solid square) trajectories as a function of the chirped laser pulse duration for the case of 90 Torr Ar gas pressure of Figure 2. Indicative error bars for the short and long trajectories are shown.

Spectral shift. The plateau harmonics are seen to suffer an overall spectral shift as the chirp of the laser pulse varies from positive to negative values. From Figure 2, where the short and long trajectories are more distinctly spectrally separated, it is evident that the long trajectory is more blue-shifted compared to the short one. This is a well-known behaviour which has been reported in the literature [11,20–22] and appears in our measurements. A very interesting characteristic, evident in both Figures 2 and 3, is that the spectral blue shift suffers a rapid change around the area of low-value negatively chirped laser pulses (<-43 fs). This fact is seen to be closely related to the initiation of intense plasma formation in these conditions. As a quantitative result, in Figure 6 we show the overall spectral shift of the 17th, 19th, and 21st high-order harmonics of Figure 3 as a function of the laser chirp for the Ar gas pressure of 80 Torr.

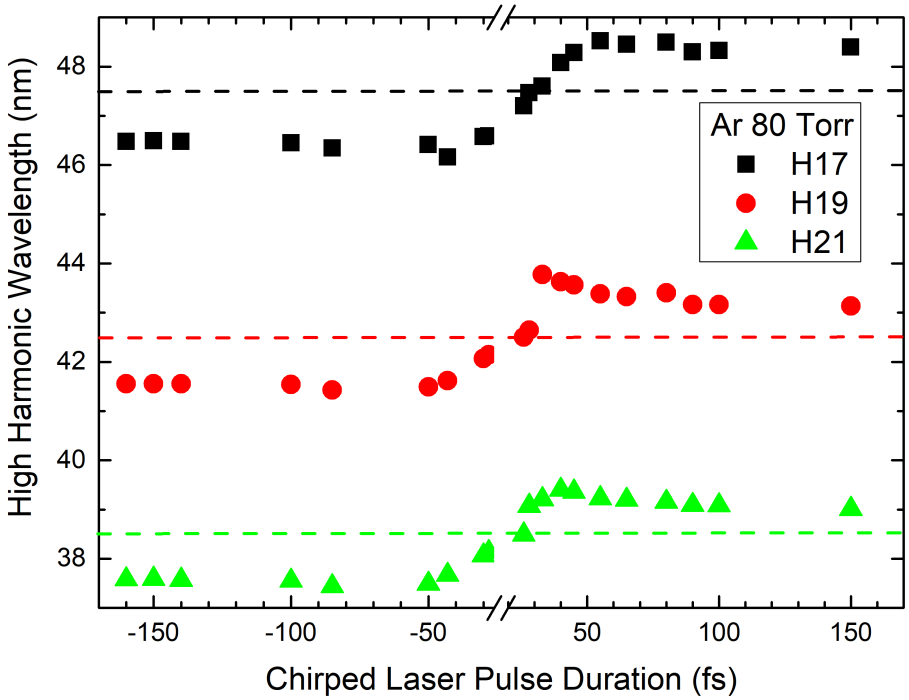

Figure 6. Experimentally determined spectral shift of the 17th (black solid square), 19th (red solid cirlce), and 21st (green solid triangle) high-order harmonics as a function of the chirped laser pulse duration for the pressure of 80 Torr of Figure 3. Dashed horizontal lines correspond to the unshifted harmonic peak positions. Estimated error bars are within the data symbols.

Wavelength tunability. Based on the above observations, HHG can be treated as a secondary coherent XUV source of tunable wavelength, the tunability of which is based on: (a) the blue shift of a harmonic as the chirp varies from positive to negative values; (b) the broadening of the HHG lines and the appearance of XUV spectral bands between the harmonics, thus forming quasi-continuum spectra.

The above qualitative features of the XUV spectral images call for their thorough understanding and interpretation. Aside from the per se interest in the fundamental physical mechanisms and balanced dynamics involved, the efficient control of the HHG characteristics is vital for a reliable and versatile coherent XUV source appropriate for use in CDI applications. In addition, the aforementioned wavelength tunability combined with the selection of the long or short trajectory is a unique feature for this XUV source. These aspects will be presented in detail in the next session.

4. Discussion

For an intense laser pulse, i.e., a laser pulse where the HHG process is not restricted to its higher intensity values at the peak of the pulse envelope, the variation of its chirp corresponds to a variation of the temporal window of the laser pulse in which the HHG is conducted. In more detail, for negatively chirped pulses, HHG is taking place mainly at the leading edge of the pulse, since at higher intensities the competing process of ionisation prevails, as evident from the intense plasma formation images shown in Figures 2 and 3. Therefore, HHG conditions are largely affected by the slope of the temporal intensity and frequency of the laser pulse at this temporal window [15]. For positively chirped pulses, plasma formation is seen to be marginal, and thus HHG is expected to be realised over a wider temporal window of the laser pulse, which, for high positive chirp values, includes the envelope peak area. This general picture of HHG dynamics will be considered for the interpretation of our findings.

The spectral shift of the harmonic peaks is a well-known effect due to mainly two mechanisms [11,20–22]. The first mechanism is the nonadiabatic response of the electronic

dipole to the rapid change of the laser field. As the laser intensity is rising in the leading edge of the pulse, the recolliding electrons gain more energy at each successive laser field cycle. Thus, the HHG at the leading edge of the laser pulse inherently induces a blue shift [23]. Similarly, a red shift is induced at the trailing edge of the laser pulse. The second mechanism corresponds to the propagation effects of the laser pulse in the partially ionised medium, which induces a spatiotemporal variation of the refractive index [14]. When the medium is rapidly ionised and plasma formation is prominent, an overall blue shift of the laser field is induced, resulting in a blue shift of the generated harmonics. However, when the ionisation is marginal, SPM due to the Kerr effect in the atomic gas induces a positive chirp in the leading edge of the laser pulse and a negative chirp in the trailing edge of the laser pulse, which is reflected as a red and blue shift, respectively, in the harmonic peaks [15].

In more detail, for laser pulses with large positive chirp values, the degree of ionisation is barely measurable, as evident from the plasma luminescence images of Figures 2 and 3. Thus, the absence of considerable plasma formation along with the intense laser peak values results in an overall red shift for the generated harmonics (see Equation (5) in Ref. [15]). As the positive chirp values become smaller, the SPM effects in the gas medium become stronger, causing a further red shift of the generated harmonics. This behaviour changes rapidly as the laser pulse reaches positive chirp values close to the FTL duration. Then, due to the higher laser pulse intensity, the SPM effects of both the gas medium and the emerging plasma become significant, and blue shifts start to appear as the chirp values change from positive to negative. It is worth noting that the higher plasma production is observed for negatively chirped pulses with durations of ~ -40 fs due to the aforementioned SPM effects, and not for the FTL pulses. In these conditions, the medium is totally depleted, even before the laser peak intensity, and thus the XUV spatiotemporal characteristics are distorted by the strong plasma formation, as observed experimentally. For lower negative chirp values (<-85 fs), the harmonics still present a blue shift, which is understood in the above picture since the corresponding plasma images show a considerable degree of ionisation, even at these high chirp values. As a quantitative picture of the above, the overall spectral shift of the high-order 17th, 19th, and 21st harmonics are shown in Figure 6 as a function of the laser chirp for the Ar gas pressure of 80 Torr.

As mentioned in the previous section, the feature of the separation of the long and short trajectory contributions is evident from the divergence of each harmonic. Long trajectories have a larger divergence than the short, due to the fact that the recolliding electron travels longer paths in the generating medium [12]. The phenomenon is enhanced when the generating medium is partially ionised, which is the case for negatively chirped pulses in our study. In addition, for laser intensities inducing a relatively high ionisation degree of the generating medium, the central wavelength of the two trajectories is also slightly different, which leads to coherent summation for each trajectory at different wavelengths (double-peaking phenomenon) [11]. The origin of divergence of the two paths in HHG has been investigated in a number of early publications [7,9,13,24,25], while experimental methods involving interferometric methods [26], the multi-jet arrangement of two gases [27,28], and phase-locked two-colour ($\omega - 2\omega$) laser fields [5,29,30] have been developed to separate and selectively control the two trajectories.

Specifically, the spectral separation of the long and short trajectories is clearly seen in Figure 2 for positively chirped pulses. The long trajectory has a narrower bandwidth and a large divergence as opposed to the short trajectory that has a broader bandwidth and a much lower divergence. In addition, the long trajectory is blue-shifted to smaller wavelengths than the short trajectory, a fact that allows for their unambiguous identification. For negatively chirped pulses with durations close to the FTL value (<-50 fs), the spectral separation of the long and short trajectories is still evident, although it is not as large as in the cases of the positively chirped pulses. Both trajectories suffer considerable blue shift, as mentioned earlier, thus resulting in their partial spectral overlapping. At even larger negative chirp values, the blue shift of the long and short trajectories results in their

complete spectral overlap, in which, however, the large divergence of the long trajectory and the higher intensity of the short are still maintained. In general, it is evident that the signal of the short harmonic is larger than the signal of the long. Especially, for the case of the +33 fs pulse duration and the 60 Torr Ar gas pressure of Figure 2, it is seen that only the short trajectory survives in the HHG spectra. The specific importance of this result has been recently reported by our research team in reference [15]. Finally, it is worth noting that the HHG production at high positively chirped pulses is remarkably increased in the case of Figure 3 compared to Figure 2. The HHG production is maximised for Ar gas pressures between 50 and 70 Torr, while it is significantly reduced for lower and higher pressure values, respectively.

Considering now the case of Figure 3, where the spectral broadening effects are more pronounced, the observed blue shifts, line broadenings, and additional spectral band appearance for small-duration negatively chirped pulses (<−50 fs) are primarily due to the enhanced SPM effects of the generating gas and the plasma formation. This is corroborated by the corresponding plasma images of Figure 3, where the highest plasma production occurs for low-value negative chirps and high-value pressures. Towards a deeper investigation of our results, we made use of our recently reported model calculations, which qualitatively supported our earlier findings [15]. Here, we adjusted the model parameters to some representative HHG conditions, i.e., for chirped laser pulses of −150 fs, −43 fs, and +150 fs at an Ar gas pressure of 60 Torr, where the spectral and divergence characteristics are reasonably distinctive. The results of the model calculations are presented in comparison to their corresponding spectral images in Figure 7. It is seen that the calculations fairly reproduce the main qualitative characteristics of the measured spectral images as they predict: (a) the marginal but evident spectral separation of the long and short trajectories for the laser pulses with durations of −150 fs; (b) the broader spectral lines and the spectral overlapping between the short and long trajectories for the laser pulses with durations of +150 fs; and (c) the line broadening and the appearance of additional spectral bands in between the harmonics' spectral locations for the laser pulses with durations of −43 fs (harmonic line distortion inside the fully ionised medium), thus resembling a quasi-continuum spectrum.

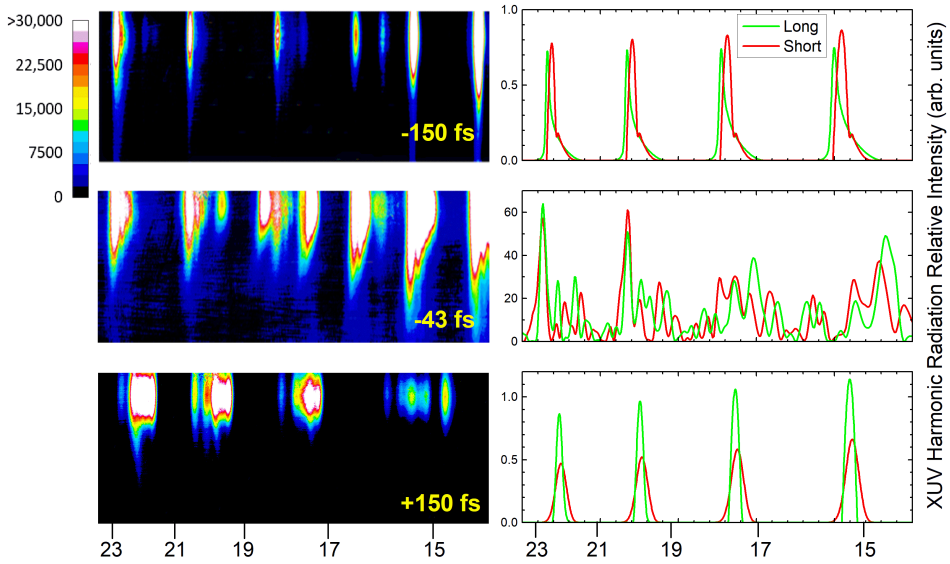

Figure 7. Qualitative comparison between measured XUV harmonic spectral images for chirped laser pulse durations of −150 fs, −43 fs, and +150 fs, corresponding to those presented in Figure 3, and XUV harmonic spectra obtained with our model calculations, corresponding to the experimental conditions of their counterpart XUV harmonic spectral images. Long and short trajectory contributions are included separately.

5. Conclusions

Based on the above analysis and discussion, it becomes clear that the frequency chirp of the fs laser pulses is a convenient and practical parameter for controlling the spatiotemporal properties of the HHG spectra, since it can be easily and accurately adjusted by detuning the ultrafast laser compressor gratings. This control of the HHG conditions and subsequent spatiotemporal characteristics of the HHG spectra is vital for a reliable secondary HHG source. The use of a semi-infinite cell as a generating medium for the secondary HHG source favours the above conditions. The gas pressure is maintained constant and can be varied at will, while the geometry of the generating gas medium can be controlled according to the laser beam focusing conditions, thus affecting the plasma formation geometry and the subsequent phase matching conditions. Our method, presented initially in reference [15] and applied here, is adding to previously reported methods [5,9,26–30] that have been proposed in the literature. It has the novel features of controlled wavelength tunability, based on the effects of blue-shift and quasi-continuum generation, as well as the separation of the short and long trajectories. Such a coherent XUV source significantly favours CDI applications in the scale of a few-tenths of nanometers [5]. Moreover, our method is expected to attract the interest of the new-generation high-average-power MHz-amplified fs laser systems, which is the new trend for high-average-power XUV high-harmonic sources.

Author Contributions: Conceptualisation, E.P.B. and N.A.P.; methodology, S.P., E.P.B. and N.A.P.; software, S.P.; validation, S.P., M.B. and M.T.; formal analysis, S.P.; investigation, S.P.; resources, E.P.B., N.A.P. and M.T.; data curation, E.P.B., N.A.P. and S.P.; writing—original draft preparation, E.P.B. and N.A.P.; writing—review and editing, E.P.B., N.A.P., M.B., S.P. and M.T.; visualisation, E.P.B. and N.A.P.; supervision, E.P.B. and N.A.P.; project administration, N.A.P.; funding acquisition, M.T., M.B., and N.A.P. All authors have read and agreed to the published version of the manuscript.

Funding: This research has been co-financed by the European Regional Development Fund of the European Union and Greek national funds through the Operational Program Competitiveness, Entrepreneurship and Innovation, under the call RESEARCH–CREATE–INNOVATE (project code: T1EDK-04549, project title: Development of a Coherent X-ray Multispectral Microscopy System).

Institutional Review Board Statement: Not applicable.

Informed Consent Statement: Not applicable.

Data Availability Statement: The data that support the findings of this study are available from the corresponding authors upon reasonable request.

Conflicts of Interest: The authors declare no conflict of interest.

References

1. Sandberg, R.L.; Paul, A.; Raymondson, D.A.; Hädrich, S.; Gaudiosi, D.M.; Holtsnider, J.; Tobey, R.I.; Cohen, O.; Murnane, M.M.; Kapteyn, H.C.; et al. Lensless Diffractive Imaging Using Tabletop Coherent High-Harmonic Soft-X-Ray Beams. *Phys. Rev. Lett.* **2007**, *99*, 098103. [CrossRef] [PubMed]
2. Zurch, M.; Rothhardt, J.; Hadrich, S.; Demmler, S.; Krebs, M.; Limpert, J.; Tunnermann, A.; Guggenmos, A.; Kleineberg, U.; Spielmann, C. Real-time and Sub-wavelength Ultrafast Coherent Diffraction Imaging in the Extreme Ultraviolet. *Sci. Rep.* **2014**, *4*, 7356. [CrossRef] [PubMed]
3. Miao, J.; Ishikawa, T.; Robinson, I.K.; Murnane, M.M. Beyond crystallography: Diffractive imaging using coherent X-ray light sources. *Science* **2015**, *348*, 530–535. [CrossRef] [PubMed]
4. Gardner, D.F.; Tanksalvala, M.; Shanblatt, E.R.; Zhang, X.; Galloway, B.R.; Porter, C.L.; Karl, R., Jr.; Bevis, C.; Adams, D.E.; Kapteyn, H.C.; et al. Subwavelength coherent imaging of periodic samples using a 13.5 nm tabletop high-harmonic light source. *Nat. Photonics* **2017**, *11*, 259–263. [CrossRef]
5. Roscam Abbing, S.; Campi, F.; Sajjadian, F.S.; Lin, N.; Smorenburg, P.; Kraus, P.M. Divergence Control of High-Harmonic Generation. *Phys. Rev. Appl.* **2020**, *13*, 054029. [CrossRef]
6. Corkum, P.B. Plasma perspective on strong field multiphoton ionization. *Phys. Rev. Lett.* **1993**, *71*, 1994–1997. [CrossRef]
7. Lewenstein, M.; Balcou, P.; Ivanov, M.Y.; L'Huillier, A.; Corkum, P.B. Theory of high-harmonic generation by low-frequency laser fields. *Phys. Rev. A* **1994**, *49*, 2117–2132. [CrossRef]
8. Ammosov, M.V.; Delone, N.B.; Krainov, V.P. Tunnel ionization of complex atoms and of atomic ions in an alternating electromagnetic field. *Soviet Phys. JETP* **1986**, *64*, 1191.

9. Salières, P.; L'Huillier, A.; Lewenstein, M. Coherence Control of High-Order Harmonics. *Phys. Rev. Lett.* **1995**, *74*, 3776–3779. [CrossRef]
10. Balcou, P.; Sali'eres, P.; L'Huillier, A.; Lewenstein, M. Generalized phase-matching conditions for high harmonics: The role of field-gradient forces. *Phys. Rev. A* **1997**, *55*, 3204–3210. [CrossRef]
11. Papadogiannis, N.; Kalpouzos, C.; Goulielmakis, E.; Nersisyan, G.; Charalambidis, D.; Auge, F.; Weihe, F.; Balcou, P. Kilohertz extreme-ultraviolet light source based on femtosecond high-order harmonic generation from noble gases. *Appl. Phys. B* **2001**, *73*, 687–692. [CrossRef]
12. Carlström, S.; Preclíková, J.; Lorek, E.; Larsen, E.W.; Heyl, C.M.; Paleček, D.; Zigmantas, D.; Schafer, K.J.; Gaarde, M.B.; Mauritsson, J. Spatially and spectrally resolved quantum path interference with chirped driving pulses. *New J. Phys.* **2016**, *18*, 123032. [CrossRef]
13. Salières, P.; Carré, B.; Le Déroff, L.; Grasbon, F.; Paulus, G.G.; Walther, H.; Kopold, R.; Becker, W.; Milošević, D.B.; Sanpera, A.; et al. Feynman's Path-Integral Approach for Intense-Laser-Atom Interactions. *Science* **2001**, *292*, 902–905. [CrossRef] [PubMed]
14. Wahlström, C.G.; Larsson, J.; Persson, A.; Starczewski, T.; Svanberg, S.; Salières, P.; Balcou, P.; L'Huillier, A. High-order harmonic generation in rare gases with an intense short-pulse laser. *Phys. Rev. A* **1993**, *48*, 4709–4720. [CrossRef]
15. Petrakis, S.; Bakarezos, M.; Tatarakis, M.; Benis, E.P.; Papadogiannis, N.A. Electron quantum path control in high harmonic generation via chirp variation of strong laser pulses. *Sci. Rep.* **2021**, *11*, 23882. [CrossRef]
16. Kim, J.H.; Nam, C.H. Plasma-induced frequency chirp of intense femtosecond lasers and its role in shaping high-order harmonic spectral lines. *Phys. Rev. A* **2002**, *65*, 033801. [CrossRef]
17. Cao, W.; Laurent, G.; Jin, C.; Li, H.; Wang, Z.; Lin, C.D.; Ben-Itzhak, I.; Cocke, C.L. Spectral splitting and quantum path study of high-harmonic generation from a semi-infinite gas cell. *J. Phys. At. Mol. Opt. Phys.* **2012**, *45*, 074013. [CrossRef]
18. Clark, E.L.; Grigoriadis, A.; Petrakis, S.; Tazes, I.; Andrianaki, G.; Skoulakis, A.; Orphanos, Y.; Kaselouris, E.; Fitilis, I.; Chatzakis, J.; et al. High-intensity laser-driven secondary radiation sources using the ZEUS 45 TW laser system at the Institute of Plasma Physics and Lasers of the Hellenic Mediterranean University Research Centre. *High Power Laser Sci. Eng.* **2021**, *9*, e53. [CrossRef]
19. Available online: https://henke.lbl.gov (accessed on 16 May 2022).
20. Shin, H.J.; Lee, D.G.; Cha, Y.H.; Hong, K.H.; Nam, C.H. Generation of Nonadiabatic Blueshift of High Harmonics in an Intense Femtosecond Laser Field. *Phys. Rev. Lett.* **1999**, *83*, 2544–2547. [CrossRef]
21. Lee, D.G.; Kim, J.H.; Hong, K.H.; Nam, C.H. Coherent Control of High-Order Harmonics with Chirped Femtosecond Laser Pulses. *Phys. Rev. Lett.* **2001**, *87*, 243902. [CrossRef]
22. Bian, X.B.; Bandrauk, A.D. Spectral Shifts of Nonadiabatic High-Order Harmonic Generation. *Appl. Sci.* **2013**, *3*, 267–277. [CrossRef]
23. Watson, J.B.; Sanpera, A.; Burnett, K. Pulse-shape effects and blueshifting in the single-atom harmonic generation from neutral species and ions. *Phys. Rev. A* **1995**, *51*, 1458–1463. [CrossRef] [PubMed]
24. Lewenstein, M.; Salières, P.; L'Huillier, A. Phase of the atomic polarization in high-order harmonic generation. *Phys. Rev. A* **1995**, *52*, 4747–4754. [CrossRef] [PubMed]
25. Gaarde, M.B.; Salin, F.; Constant, E.; Balcou, P.; Schafer, K.J.; Kulander, K.C.; L'Huillier, A. Spatiotemporal separation of high harmonic radiation into two quantum path components. *Phys. Rev. A* **1999**, *59*, 1367–1373. [CrossRef]
26. Bellini, M.; Lyngå, C.; Tozzi, A.; Gaarde, M.B.; Hänsch, T.W.; L'Huillier, A.; Wahlström, C.G. Temporal Coherence of Ultrashort High-Order Harmonic Pulses. *Phys. Rev. Lett.* **1998**, *81*, 297–300. [CrossRef]
27. Willner, A.; Tavella, F.; Yeung, M.; Dzelzainis, T.; Kamperidis, C.; Bakarezos, M.; Adams, D.; Schulz, M.; Riedel, R.; Hoffmann, M.C.; et al. Coherent Control of High Harmonic Generation via Dual-Gas Multijet Arrays. *Phys. Rev. Lett.* **2011**, *107*, 175002. [CrossRef]
28. Willner, A.; Tavella, F.; Yeung, M.; Dzelzainis, T.; Kamperidis, C.; Bakarezos, M.; Adams, D.; Riedel, R.; Schulz, M.; Hoffmann, M.C.; et al. Efficient control of quantum paths via dual-gas high harmonic generation. *New J. Phys.* **2011**, *13*, 113001. [CrossRef]
29. Ishii, N.; Kosuge, A.; Hayashi, T.; Kanai, T.; Itatani, J.; Adachi, S.; Watanabe, S. Quantum path selection in high-harmonic generation by a phase-locked two-color field. *Opt. Express* **2008**, *16*, 20876–20883. [CrossRef]
30. Brugnera, L.; Hoffmann, D.J.; Siegel, T.; Frank, F.; Zaïr, A.; Tisch, J.W.G.; Marangos, J.P. Trajectory Selection in High Harmonic Generation by Controlling the Phase between Orthogonal Two-Color Fields. *Phys. Rev. Lett.* **2011**, *107*, 153902. [CrossRef]